The American Journal of Pathology, Vol. 171, No. 2, August 2007

DOI: 10.2353/ajpath.2007.061044

Stem Cells, Tissue Engineering and Hematopoietic Elements

Population Control of Resident and Immigrant Microglia by Mitosis and Apoptosis

Martin Wirenfeldt,* Lasse Dissing-Olesen,* Alicia Anne Babcock,* Marianne Nielsen,† Michael Meldgaard,* Jens Zimmer,† Iñigo Azcoitia,‡ Robert Graham Quinton Leslie,§ Frederik Dagnaes-Hansen,¶ and Bente Finsen*

From the Medical Biotechnology Center and the Departments of Anatomy and Neurobiology† and Immunology and Microbiology,§ Institute of Medical Biology, University of Southern Denmark, Odense, Denmark; the Department of Medical Microbiology and Immunology,¶ University of Aarhus, Aarhus, Denmark; and the Departamento de Biología Celular,‡ Facultad de Biología, Universidad Complutense, de Madrid, Madrid, Spain*

Microglial population expansion occurs in response to neural damage via processes that involve mitosis and immigration of bone marrow-derived cells. However, little is known of the mechanisms that regulate clearance of reactive microglia, when microgliosis diminishes days to weeks later. We have investigated the mechanisms of microglial population control in a well-defined model of reactive microgliosis in the mouse dentate gyrus after perforant pathway axonal lesion. Unbiased stereological methods and flow cytometry demonstrate significant lesion-induced increases in microglial numbers. Reactive microglia often occurred in clusters, some having recently incorporated bromodeoxyuridine, showing that proliferation had occurred. Annexin V labeling and staining for activated caspase-3 and terminal deoxynucleotidyl transferase-mediated dUTP nick end-labeling showed that apoptotic mechanisms participate in dissolution of the microglial response. Using bone marrow chimeric mice, we found that the lesion-induced proliferative capacity of resident microglia superseded that of immigrant microglia, whereas lesion-induced kinetics of apoptosis were comparable. Microglial numbers and responses were severely reduced in bone marrow chimeric mice. These results broaden our understanding of the microglial response to neural damage by demonstrating that simultaneously occurring mitosis and apoptosis regulate expansion and reduction of both resident and immigrant microglial cell populations. ***(Am J Pathol 2007, 171:617–631; DOI: 10.2353/ajpath.2007.061044)***

Microglia represent the first line of defense against pathogens or injury in the central nervous system (CNS).[1] By dynamically surveying the CNS, microglia serve important maintenance functions for neurons, with which they have intimate contact.[2,3] Key functions include metabolism of nucleosides and purines,[2,3] phagocytosis, and production of growth factors and cytokines.[4,5] The significance of microglial function in maintaining CNS homeostasis is evident from the discovery that individuals with loss of function mutations of the TREM2/DAP12 receptor complex, which renders microglia unable to phagocytose apoptotic neurons in mice,[6] develop symptoms of presenile dementia.[7]

Microglia are unique cells in the CNS parenchyma, being innate immune cells and having a mesodermal origin. In line with their myeloid lineage,[8] slow microglial turnover in normal CNS[9] and enhanced recruitment during reactive microgliosis[10,11] indicate that microglia are potentially replaceable cells, making microglia and their myeloid progenitors promising candidates for active cellular therapy in CNS disease and injury.[12,13] For potential microglial cell therapy to be safe and applicable for the treatment of neurological disease, information is needed about the population control of immigrating microglia that become involved in the microglial reaction.

Supported by the Familien Hede Nielsens Fond, Augustinus Fonden, Fonden til Lægevidenskabens Fremme, Direktør Jacob Madsen and Hustru Olga Madsens Fond, A.J. Andersen og Hustrus Fond, Fhv. Direktør Leo Nielsen og Hustru Karen Margrethe Nielsens Legat for Lægevidenskabelig Grundforskning, Overlægerådets legatudvalg, Overlæge, dr.med. Alfred Helsted og hustru dr.med. Eli Møllers legat, Civilingeniør Holger Rabitz og hustru Doris Mary, født Phillipp's Mindelegat, Mogens Svarre Mogensens Fond, Carl og Ellen Hertzs Legat til Dansk Læge-og Naturvidenskab, Dagmar Marshalls Fond, Handelsgartner Ove William Buhl Olesen og ægtefælle fru Edith Buhl Olesens Mindelegat, Gudrun Krauses Mindelegat, The Danish Medical Association Research Fund/The Johanne Dorthe Due Estate, Else Poulsens Mindelegat, Foundation for Research in Neurology, The Warwara Larsen Foundation, The Novo Nordic Foundation, The Lundbeck Foundation, The Danish Medical Research Council, and the Faculty of Health Sciences at The University of Southern Denmark.

Accepted for publication April 20, 2007.

Address reprint requests to Martin Wirenfeldt, Medical Biotechnology Center, University of Southern Denmark, Winsløwparken 25, 2, DK-5000 Odense C, Denmark. E-mail: mwirenfeldt@gmail.com.

Acute activation of microglia as a result of neural injury or pathology quickly leads to reactive microgliosis, a cardinal feature being expansion in the number of microglia in the affected region. Increase in cell number originates in part from recruitment of myeloid cells,[11] proliferation,[14] or migration from juxtaposed regions.[15] The state of reactive microgliosis dissolves days to weeks later, according to an inherently tightly regulated schedule, which has been suggested to involve microglial apoptosis.[16] The cellular population control of immigrating and resident microglia should be comparable if immigrating bone marrow (BM)-derived cells are to take part fully in regular microglial tasks.

To address these fundamental questions, we investigated whether resident and immigrating microglia are governed by similar mechanisms of population control, ie, cellular multiplication by mitosis and reduction of the cellular population by apoptosis. Reactive microgliosis was induced in the dentate gyrus and hippocampus in unmanipulated and green fluorescent protein (GFP)-BM-chimeric mice by transection of the perforant pathway (PP) projection in the entorhinal cortex. Our results show that microglial expansion is balanced by simultaneously occurring mitosis and apoptosis. The axonal lesion-induced mitotic activity of resident microglia supersedes that of BM-derived immigrant microglia, whereas the kinetics of lesion-induced apoptotic responses are comparable.

Materials and Methods

Animals

C57BL/6J mice (Taconic, Skensved, Denmark; or Harlan, Allerød, Denmark) were used for studies of nonchimeric mice. For BM-chimeric studies, C57BL/6 congenic B6.SJL-*Ptprc*^{a}*Pepc*^{b}/BoyJ mice (The Jackson Laboratory, Bar Harbor, ME), which express the CD45.1 allotype and are hence abbreviated B6(CD45.1), were used as transplant recipients and C57BL/6-Tg(UBC-GFP)30Scha/J mice (The Jackson Laboratory)[17] as BM donors. This combination of mice was chosen so that immigrating cells could be identified in chimeric mice by two criteria: positive expression of GPF and CD45.2, which is normally expressed in C57BL/6 mice. Expression of the GFP transgene, however, proved by itself to be a sufficiently strong and reliable signal. A group of nonirradiated B6(CD45.1) mice (The Jackson Laboratory) was included to control for potential differences from C57BL/6 mice. Mice were housed and bred and animal experiments performed at the Laboratory of Biomedicine at the University of Southern Denmark and at the Department of Medical Microbiology and Immunology at Aarhus University. All animal experiments were performed according to Danish law and protocols approved by the Danish Ethical Animal Care Committee.

PP Lesion

Microglial activation in the hippocampus and dentate gyrus was induced by the anterograde axonal and terminal degeneration of presynaptic elements resulting from transection of the entorhino-hippocampal PP projection,[18–21] performed as previously described.[11] Mice were anesthetized with a mixture of ketamine and xylazine (for flow cytometry) or fentanyl citrate, fluanisone, and diazepam (for histology) and fixed in a stereotaxic frame (Stoelting, Wood Dale, IL). The PP transection was made with a wire knife (David Kopf Instruments, Tujunga, CA) angled 10 degrees lateral and rotated 15 degrees rostral and the nosebar set at −3 mm. The closed wire knife was inserted 2.1 mm lateral to the lambda and 0.3 mm caudal to the lambdoid suture through a drilled trepanation. A 3.1-mm-long cut was made in the entorhinal cortex starting 3.4 mm ventral to the meninges. Mice were supplied with eye ointment and postoperative injections of saline and buprenorphine. Animals were placed in a warm environment for postoperative recovery.

BM Transplantation

Recipient mice were irradiated with 9.5 Gy in a single dose from a ^{137}Cs source (Risø National Laboratory, Roskilde, Denmark) and were reconstituted with BM cells obtained from GFP transgenic donor mice.[10,11] Donor BM cells were harvested by flushing the medullary canal of the femoral and tibial diaphysis with RPMI 1640 medium (Gibco, Paisley, UK). After centrifugation, the cell suspension was filtered and transplanted by intravenous injection. The transplanted mice were supplied with oxytetracycline (2 g/L Terramycin veterinary 20%; Pfizer, Amoise, France) in the drinking water for 3 days after transplantation.[11] Chimerism was assessed by expression of GFP in blood cells at the time of sacrifice. Positive GFP expression was determined using autofluorescence levels in blood cells from non-Tg mice as negative controls. Flow cytometric analysis showed that 91.6 ± 1.1% (mean ± SEM) of blood cells were GFP$^+$, indicating that successful reconstitution had occurred.

Real-Time Polymerase Chain Reaction (PCR)-Based Testing for UbC-GFP Zygosity

Genomic DNA was extracted from external ear tissue, obtained from labeling of animals for identity, by alkaline lysis in 0.1 mol/L KOH for 1 hour at 95°C followed by KH_2PO_4 neutralization. Extracts were diluted 20-fold, and 2 μl were applied for 25-μl real-time PCR. The reaction mixture contained 1× RealQ master (Ampliqon; Bie and Berntsen A/S, Rødovre, Denmark) and for transgene PCRs 300 nmol/L of each of the two primers (5′-ATTGTCCGCTAAATTCTGGCCGTTT/GCTCGACCAGGATGGGCACC-3′) (TAG, Copenhagen, Denmark) and SYBR Green diluted 20,000-fold. Lymphotoxin-α (LT-α) reference gene PCRs contained 400 nmol/L of the two primers (5′-GTCCAGCTCTTTTCCTCCCAAT/GTCCTTGAAGTCCCGGATACAC-3′) and 50 nmol/L TaqMan probe

(5′-CCTTCCATGTGCCTCTCCTCAGTGCG-3′). For PCR and detection in real time, an iCycler (Bio-Rad, Herlev, Denmark) was used. The thermocycling protocol was 95°C for 15 minutes to activate the RealQ enzyme followed by 40 cycles of 95°C for 15 seconds, 62°C for 30 seconds, and 72°C for 45 seconds.

Real-Time PCR-Based mRNA Analysis

RNA was extracted using RNeasy Protect mini kits (Qiagen, Hilden, Germany) or TRIzol (Invitrogen, Taastrup, Denmark), as previously described for PP-lesioned hippocampus samples.[22,23] Complementary DNA was synthesized from 0.4 μg of total RNA by reverse transcription, using previously established conditions.[23] For real-time PCR, a Bio-Rad iCycler was used. Each reaction contained a total volume of 25 μl, 5 of which were diluted cDNA. The other components were RealQ master mix (1.5 mmol/L magnesium at 1×, Ampliqon; Bie and Berntsen A/S), 1 to 2 mmol/L of additional $MgCl_2$, SYBR Green, fluorescein, and 300 nmol/L of each PCR primer. Newly designed primer sets were validated to specifically amplify the respective target only. These were M-CSF (5′-CGCTGCCCTTCTTCGACATG/ACACCTCCTTGGCAATACTCCT-3′; annealing temperature, 60°C; magnesium concentration, 3.5 mmol/L), M-CSFR (5′-GCATTACAACTGGACCTACCTA/AGAGCTTGAATGTGTACCTGTAT-3′; annealing temperature, 55°C; magnesium concentration, 3.0 mmol/L), GM-CSF, which was targeted by two different primer sets (5′-CATGTAGAGGCCATCAAAGAAG/ACGACTTCTACCTCTTCATTCAA-3′; annealing temperature, 56°C; magnesium concentration, 3.5 mmol/L; and 5′-GGGCAATTTCACCAAACTCAA/TTTCACAGTCCGTTTCCGG-3′; annealing temperature, 56°C; magnesium concentration, 3.5 mmol/L) targeting exons 1/2 and 3/4, respectively, and GM-CSFR (5′-AGTGACGTGCAGGAGGTTCG/ACGTCGTCGGACACCTTGT-3′; annealing temperature, 60°C; magnesium concentration, 3.5 mmol/L). Amplification of CD11b and HPRT1 was done using previously published primer and probe sequences, and FAM- or HEX-labeled TaqMan probes instead of SYBR Green, respectively.[23] Each cDNA was subjected to triplicate real-time PCR analysis. Calibrator samples were included on all plates. Data were normalized using HPRT1 reference gene, averaged, and calibrated against the calibrator ratio. Data are presented as relative values.

Labeling of Proliferating Cells in Vivo

For *in vivo* detection of microglial mitosis, proliferating cells were labeled with 5-bromo-2′-deoxyuridine (BrdU), which is incorporated into DNA during mitotic S phase. Each mouse was injected with a 90-mg/kg dose of BrdU dissolved in phosphate-buffered saline (PBS; 10 mg/ml) intraperitoneally three times at 8-hour intervals for the last 24 hours before perfusion. Mice used for BrdU histology were injected with 50 mg/kg 1 hour before sacrifice.

Flow Cytometry

Mice were sacrificed under pentobarbital anesthesia by exsanguination and intracardiac perfusion with 20 ml of PBS. The brains were removed, and the hippocampus and dentate gyrus were dissected out *en bloc* from the contralateral and lesioned hemispheres. These samples did not include tissue surrounding the wire knife lesion because this was in the entorhinal cortex, and any adherent choroid plexus was removed.[24] Hippocampal tissue was homogenized through a 70-μm cell strainer (BD Falcon, Franklin Lakes, NJ) in RPMI 1640 medium (Gibco) containing 10% fetal bovine serum (FBS; Gibco). After centrifugation, cells were incubated with anti-FcγIII/II receptor antibody (BD Biosciences, Erembodegem, Belgium) and 50 μg/ml of Syrian hamster Ig (Jackson Immunoresearch, West Grove, PA) in RPMI 1640 medium with 10% FBS at room temperature for 45 to 60 minutes to block nonspecific staining.[11,22]

For annexin V analysis, surface antigen labeling was performed by incubating cells for 30 minutes at room temperature with phycoerythrin (PE)-conjugated anti-CD45 antibody and fluorescein isothiocyanate-conjugated anti-CD11b (BD Biosciences) in RPMI 1640 medium with 10% FBS. For studies in chimeric mice, anti-CD11b was necessarily omitted because the FL1 channel was occupied by GFP fluorescence. Essentially all $CD45^{dim}$ cells coexpress CD11b, and relative levels of CD45 can distinguish microglia ($CD45^{dim}$) from leukocytes ($CD45^{high}$).[25–27] Cells were then washed once in RPMI 1640 medium with 10% FBS and twice in annexin V-binding buffer (10 mmol/L HEPES, 140 mmol/L NaCl, and 2.5 mmol/L $CaCl_2$, pH 7.4) before incubation for 15 minutes at room temperature in a mixture of APC-conjugated annexin V (BD Biosciences), which labels apoptotic cells, and the viability marker 7-amino-actinomycin D (7-AAD), which allows exclusion of dead cells (BD Biosciences).

For BrdU analysis, cells from chimeric and nonchimeric mice were washed in staining buffer (Hanks' balanced salt solution containing 2% FBS and 0.1% sodium azide) and for surface antigen labeling incubated with PE-conjugated anti-CD45 and PerCP-Cy5.5-conjugated anti-CD11b antibodies (BD Biosciences). Cells were then washed in staining buffer and fixed, permeabilized, and stained with APC-conjugated anti-BrdU antibody for intracellular BrdU detection according to instructions provided with the APC BrdU flow kit (BD Biosciences). All stainings were analyzed on a BD FACSCalibur flow cytometer and BD CellQuest Pro software (BD Biosciences, San Jose, CA). Isotype, antigen omission (for BrdU), and autofluorescence (for GFP, 7-AAD, and annexin V) controls served to determine fluorescence levels for positive staining. Specificity of annexin V binding was additionally tested by blocking with recombinant annexin V.

For quantification of flow cytometry data, cells were gated on side scatter (SSC) versus CD11b and SSC versus either intermediate expression of CD45 to identify parenchymal microglia ($CD45^{dim}CD11b^{+}$), or high levels of CD45 to identify macrophages ($CD45^{high}CD11b^{+}$). Note that identification of apoptotic microglia in chimeric

mice was based solely on SSC versus $CD45^{dim}$ expression for reasons outlined above. All microglia/macrophages included in annexin V analyses were additionally gated to show only viable cells, by excluding late apoptotic and necrotic cells positive for 7-AAD from the analysis. Note that certain flow cytometry profiles included in figures are shown for descriptive purposes only, and may have alternate gating strategies; this information is specified in the figure legends.

Numbers of microglia or macrophages in one hippocampus were calculated as the number of gated $CD45^{dim}CD11b^{+}$ microglia or gated $CD45^{high}CD11b^{+}$ macrophages multiplied by the reciprocal fraction of the sample volume used and multiplied by two. This last step was taken because each hippocampal sample was split in two, ie, half was used for annexin V analysis and the other half for BrdU incorporation. For C57BL/6 mice, the data are presented as the average of these duplicates. For chimeric mice, the data are presented from our analysis of BrdU-stained cells because both CD45 and CD11b antibodies could only be included there. Note that number data generated from groups of B6(CD45.1) and C57BL/6 mice used for comparison with chimeric mice were also estimated using this approach. Numbers of microglial and macrophage subpopulations were calculated by applying the proportion of the subset to the total number estimate. Preparation and staining of hippocampal homogenate inevitably leads to cells loss, and the cell numbers and proportions presented are based on cells remaining in suspension.

Histology

For stereological quantification of total microglial numbers in the dentate gyrus, vibratome sections were processed for immunohistochemical visualization of $CD11b^{+}$ microglia. PP-lesioned mice were sacrificed under pentobarbital anesthesia by exsanguination and intracardiac perfusion with 5 ml of Sørensen's phosphate buffer (25 mmol/L KH_2PO_4 and 125 mmol/L Na_2HPO_4, pH 7.4) followed by 20 ml of Sørensen's phosphate buffer containing 4% paraformaldehyde. The brains were additionally fixed 1 hour in Sørensen's phosphate buffer containing 4% paraformaldehyde on ice and 21 hours in Sørensen's phosphate buffer with 1% paraformaldehyde at 4°C. Sections of 70-μm thickness were cut on a VT1000S vibratome (Leica, Nussloch, Germany) and transferred to de Olmos cryoprotectant solution [10 g of polyvinylpyrrolidone (Sigma-Aldrich, Brondby, Denmark) and 300 g of sucrose diluted in a mixture of 300 ml of ethyleneglycol (Merck, Glostrup, Denmark) and 700 ml of $NaPO_4$ buffer] for long-term storage. Sections selected for CD11b labeling were rinsed in Tris-buffered saline (TBS; 50 mmol/L Trisma base and 110 mmol/L NaCl, pH 7.4), endogenous peroxidase activity was blocked in methanol containing 0.6% H_2O_2 for 10 minutes at room temperature, and sections were incubated in staining buffer (TBS containing 1% Triton X-100 and 10% FBS) for 1 hour at room temperature. Incubation with the anti-CD11b antibody (Serotec, Hamar, Norway) in staining buffer was done overnight at 4°C. Subsequent incubations with secondary goat anti-rat biotinylated antibody (Amersham Biosciences, Little Chalfont, UK) and horseradish peroxidase conjugated streptavidin in staining buffer were performed at room temperature for 1 hour. Labeling was visualized with 3,3′-diaminobenzidine, and sections were mounted on gelatinized microscope slides, dried overnight, stained with toluidine blue, dehydrated in graded ethanol, cleared in xylene, and coverslipped in Depex mounting medium.

Visualization of apoptotic $CD11b^{+}$ microglia expressing activated caspase-3 was done in 16-μm-thick cryostat sections mounted on microscope slides. Tissue sections were rinsed in TBS and in TBS containing 1% Triton X-100 (TBS-T) before incubation in staining buffer for 1 hour at room temperature. The tissue was subsequently incubated with rat anti-mouse CD11b antibody (Serotec) and rabbit anti-human activated caspase-3 antibody (Cell Signaling Technology, Boston, MA) diluted in staining buffer overnight at 4°C. Afterward the tissue was rinsed in TBS-T and incubated with Alexa Fluor 568-conjugated goat anti-rat IgG antibody (Invitrogen) and Alexa Fluor 488-conjugated goat anti-rabbit IgG antibody (Invitrogen). The tissue was finally rinsed in TBS and stained with 4′,6-diamidino-2-phenylindole (DAPI). After a final rinse in TBS, sections were coverslipped in Prolong Gold anti-fade medium (Invitrogen). Visualization of activated caspase-3-positive cells in the free-floating vibratome sections was done as described for CD11b using 3,3′-diaminobenzidine as chromogen.

Fragmented DNA in apoptotic microglia was visualized applying terminal deoxynucleotidyl transferase-mediated dUTP nick end-labeling (TUNEL) together with CD11b and DAPI staining. Free-floating 70-μm-thick vibratome sections were rinsed in TBS and TBS-T before preincubation in staining buffer at room temperature and incubation with CD11b antibody (Serotec) at 4°C overnight. Sections were then rinsed in TBS-T and incubated for 1 hour at room temperature with an Alexa Fluor 568-conjugated goat anti-rat IgG antibody. After rinsing in TBS-T fluorescein isothiocyanate-conjugated dUTP nick end labeling was performed according to kit instructions (Roche Diagnostics, Hvidovre, Denmark). Finally, sections were rinsed in PBS, mounted on gelatinized microscope slides, dried, stained with DAPI, and coverslipped in Prolong Gold anti-fade medium.

For confocal analysis of microglial clusters, free-floating 70-μm-thick vibratome sections were rinsed in TBS and TBS-T before preincubation in staining buffer at room temperature. The tissue was then incubated with rat anti-mouse CD11b antibody (Serotec) overnight at 4°C. Sections were rinsed in TBS-T and incubated for 1 hour at room temperature with Alexa Fluor 488 conjugated goat anti-rat IgG antibody. Sections were then rinsed in TBS and stained with propidium iodide. After a final rinse in TBS, the sections were mounted in TBS and coverslipped using Gerbatol mounting medium. Fluorescence stainings were analyzed using a Leica TCS 4D/DM IRB laser-scanning confocal microscope.

For visualization of mitotic microglia, 16-μm-thick cryostat sections were rinsed in TBS and in TBS-T before

immersion in 1 mol/L HCl for 10 minutes on ice, 2 mol/L HCl for 10 minutes at room temperature, and 2 mol/L HCl for 20 minutes at 37°C. Tissue was rinsed in TBS-T and incubated with staining buffer for 1 hour at room temperature followed by incubation with biotinylated tomato lectin (Sigma, Copenhagen, Denmark) and rat anti-BrdU antibody (Abcam, Cambridge, UK) diluted in staining buffer at 4°C overnight. The tissue was then rinsed in TBS-T and incubated with Alexa Fluor 568-conjugated goat anti-rat IgG antibody and Alexa Fluor 488-conjugated streptavidin. The tissue was finally rinsed in TBS and stained with DAPI, and sections were coverslipped in Prolong Gold anti-fade medium.

In situ visualization of GFP^+ BM-derived microglia was done in 16-μm-thick cryostat sections. Sections were rinsed in TBS before preincubation in TBS containing 10% FBS for 1 hour. The tissue was incubated overnight with rat anti-mouse CD11b antibody (Serotec) in TBS containing 10% FBS and 0.5% Triton X-100. The sections were subsequently rinsed in TBS and incubated with an Alexa Fluor 568-conjugated rabbit anti-rat IgG antibody for 1 hour, rinsed again in TBS, and coverslipped in Prolong Gold anti-fade medium with DAPI. Fluorescence stainings were analyzed using an Olympus BX51 fluorescence microscope and DP70 digital color camera.

Stereology

Histological quantification of microglia was based on the protocol for counting neurons in the hippocampus, by applying the optical fractionator[28] adapted for unbiased counting of microglia in the dentate gyrus as previously described.[29] All counting was performed using the computer-assisted stereological toolbox (CAST)-Grid software (Visiopharm, Hørsholm, Denmark) connected to an Olympus BX50 microscope equipped with motorized stage and focus units. Each brain was sectioned horizontally in four parallel series of sections. One was used for stereological counting giving a section sampling fraction ssf of 1/4. Cells were sampled in counting frames of 644 to 988 μm^2 [a(frame)] moved in *x* and *y* steps of 100 μm $\times$ 100 μm [a(step)]. The area sampling fraction asf was calculated as a(frame)/a(step). The thickness sampling fraction tsf was calculated as the height of the optical disector probe h (8 or 10 μm) divided by the average height of the sections t (tsf = h/t). Total cell number *N* was estimated using the equation: $N = \Sigma Q^- \cdot 1/tsf \cdot 1/asf \cdot 1/ssf$, ΣQ^- being the number of cells counted. In the case of microglial clusters, each cluster was counted as one cell and identified by the most clearly defined nucleus. Coefficients of error and variation were calculated,[28] as previously described.[29]

Statistics

Data are presented as mean ± SEM. Groups of contralateral and deafferented hippocampi were analyzed with a paired *t*-test. For comparison of the proportions of GFP^+ immigrant microglia between the contralateral and lesioned hippocampi, the level of statistical significance was set at a one-tailed *P* value of <0.05. The level of statistical significance for other analyses was set at a two-tailed *P* value of <0.05. For comparison of three or more groups, a one-way analysis of variance was applied and individual groups compared using Bonferroni's post test. *P* values are indicated as follows: $*P < 0.05$, $**P < 0.01$, and $***P < 0.001$.

Results

Reactive Changes in the $CD11b^+$ Microglial Population in the Dentate Gyrus and Hippocampus

The degeneration of the PP axons and their presynaptic terminals induced reactive microgliosis in the deafferented areas of the dentate gyrus and hippocampus (Figure 1), as previously described.[30–32] Reactive microgliosis was observed in the PP termination areas in the outer part of the dentate molecular layer, the CA3 stratum moleculare, and the stratum lacunosum moleculare of the ipsi- and contralateral CA1 (Figure 1), the latter attributable to transection of the ipsilateral and crossed temporoammonic tracts.[33] Microglial activation was therefore also observed in white matter in the alveus and fimbria fornix attributable to degeneration of transected commissural axons (Figure 1). Three days later, microglia had acquired a characteristic dense hyperramified morphology and formed distinct clusters of reactive cells throughout the deafferented areas (Figure 2, A and B). At 5 and 7 days after lesion, the microglial reaction was almost confluent and separation of individual microglial cells unclear (Figure 2B). Using confocal laser-scanning microscopy on clusters identified by immunofluorescence staining for CD11b and propidium iodide as a nuclear marker, it was determined that these clusters represented aggregates of microglial cells, ie, nuclei separated by a rim of CD11b-stained plasma membrane (Figure 2C). Analysis of ~50 microglial clusters revealed that most clusters represented two reactive microglial cells, but clusters consisting of three to four cells were also observed (Figure 2C, displayed 3 days after lesion).

Axonal Lesion-Induced Increase in Microglial Numbers

A cardinal feature of reactive microgliosis after PP lesion is microglial mitosis giving rise to an increase in the number of microglia in the deafferented area.[14,34] We have previously used stereological methods to estimate that there are 12,300 resting, ramified $CD11b^+$ microglia in the molecular and granular cell layer of the dentate gyrus of normal mice.[29] Similar numbers have been generated by others.[35] Here, the same method was applied to estimate the total number of reactive microglia in the molecular and granular cell layer of the deafferented dentate gyrus. Numbers of microglia were significantly increased 3, 5, and 7 days after PP transection (22,700,

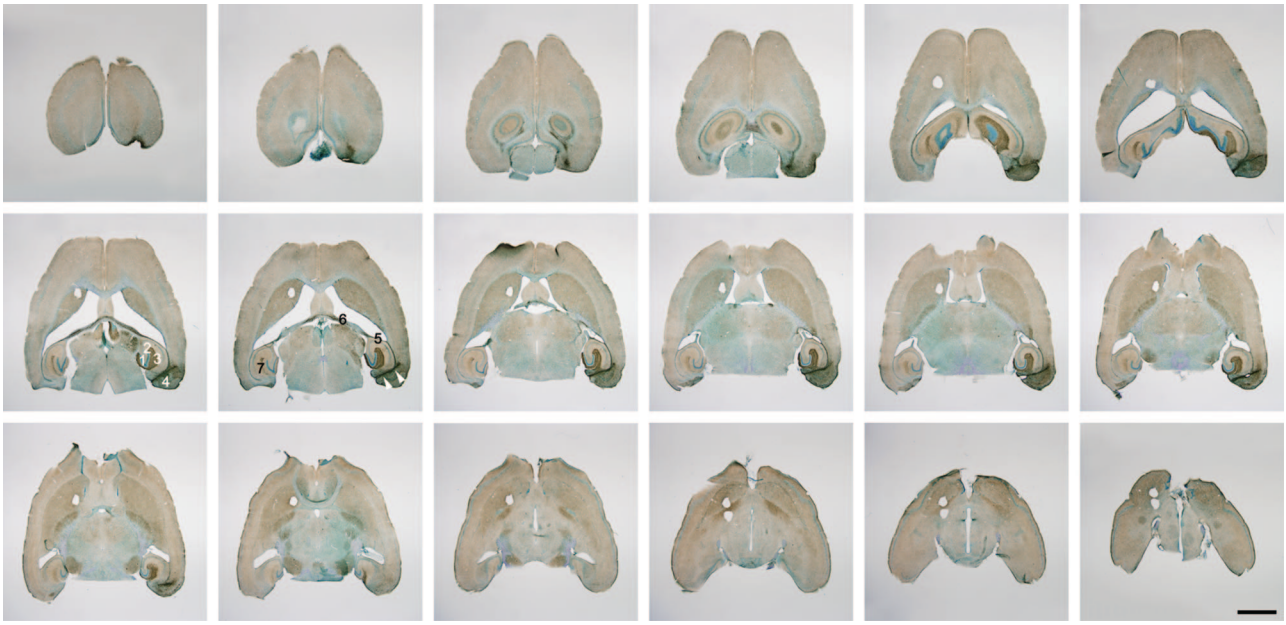

Figure 1. Low-power micrographs of CD11b-stained sections sampled for stereological estimation of total microglial numbers in the hippocampal dentate gyrus from PP lesioned mouse 7 days after lesion. The 70-μm-thick counterstained sections are equally spaced 280 μm apart. Reactive microgliosis is observed in the areas of PP termination in the outer two-thirds of the dentate gyrus molecular layer, the CA3 stratum moleculare, and the stratum lacunosum-moleculare of the CA1 ipsi- and contralaterally. Microglial activation can additionally be observed in white matter in the alveus and fimbria fornix. The wire-knife transection site in the entorhinal cortex is indicated by **arrowheads**. 1, dentate gyrus; 2, hippocampal CA3 region; 3, hippocampal CA1 region; 4, entorhinal cortex; 5, alveus; 6, fornix; 7, stratum lacunosum-moleculare in contralateral CA1. Scale bar = 2 mm.

22,400, and 24,100, respectively) versus previously generated microglial numbers 12,300 in unmanipulated mice.[29] Comparison of the groups with 3-, 5-, or 7-day survival after lesion showed no statistically significant differences between groups (Table 1), indicating that there was no clear peak in numerical expansion in the dentate gyrus at these times. Reactive microglia that occurred in multicellular clusters (Figure 2, B and C) were necessarily counted as a single cell, because individual cells within the clusters could not easily be resolved by conventional light microscopy. This probably underestimated the total number of microglia in the deafferented dentate gyrus, as well as the fold increase compared with unmanipulated dentate gyrus, where only individual resting microglia were observed. To determine the proportion of clustered microglia, microglial counts were classified in three categories: 1) reactive microglia with one nucleus; 2) microglial clusters; and 3) resting, ramified microglia (Table 2). Depending on the survival time after lesion, microglial clusters constituted 72 to 76% of the counted microglia. The actual number of microglia could then potentially be twofold higher or even more than the estimates listed in Table 1.

Although microglia is the most prominent myeloid cell population in the PP-deafferented dentate gyrus, CD11b has been shown to additionally stain several smaller populations of myeloid cells after PP lesion.[10,11,22] By flow cytometry, microglia and macrophages can be identified and quantified based on their expression of CD45 and CD11b, as illustrated in the flow cytometry dot plots in Figure 3A. Resting and reactive microglia express CD11b ($CD11b^+$) and intermediate levels of CD45 ($CD45^{dim}$) and are hence referred to as $CD45^{dim}CD11b^+$, whereas macrophages express considerably higher levels of CD45 ($CD45^{high}CD11b^+$). The dot plots that resulted from analysis of isolated whole hippocampus including the dentate gyrus indicate that the number of microglia increased 3 and 7 days after lesion and that macrophages contributed to the response, especially at 3 days after lesion (Figure 3A). This is consistent with previous flow cytometry studies showing that whereas microglial proportions increase between 2 and 5 days after lesion, macrophage proportions decline.[22,24] This lesion-induced increase in microglial and macrophage numbers in the hippocampus was quantified. Because a known fraction of hippocampal cells were analyzed by flow cytometry, this allowed for estimation of the total number of microglia and macrophages from unlesioned and contralateral and deafferented hippocampi at different times after lesion (Figure 3). Number estimates generated from flow cytometric analyses include deafferented as well as unaffected hippocampal subregions and reflect inevitable cell loss during the preparation and staining of cell suspensions. Numbers of microglia increased 3, 7, 14, and 28 days after PP transection (41,000, 38,900, 30,100, and 31,100, respectively), compared with unlesioned mice (20,300) (Figure 3B). As with our stereological estimates, no significant difference was detected in deafferented hippocampus between 3 and 7 days. By 14 days, however, microglial numbers had begun to decline. For macrophages, the lesion-induced increase in numbers was only observed 3, 7, and 14 days after lesion (Figure 3C). Three days after lesion only 750 macrophages were present in deafferented hippocampus compared with 41,000 microglia (<2%; Figure 3, B and C). Significantly

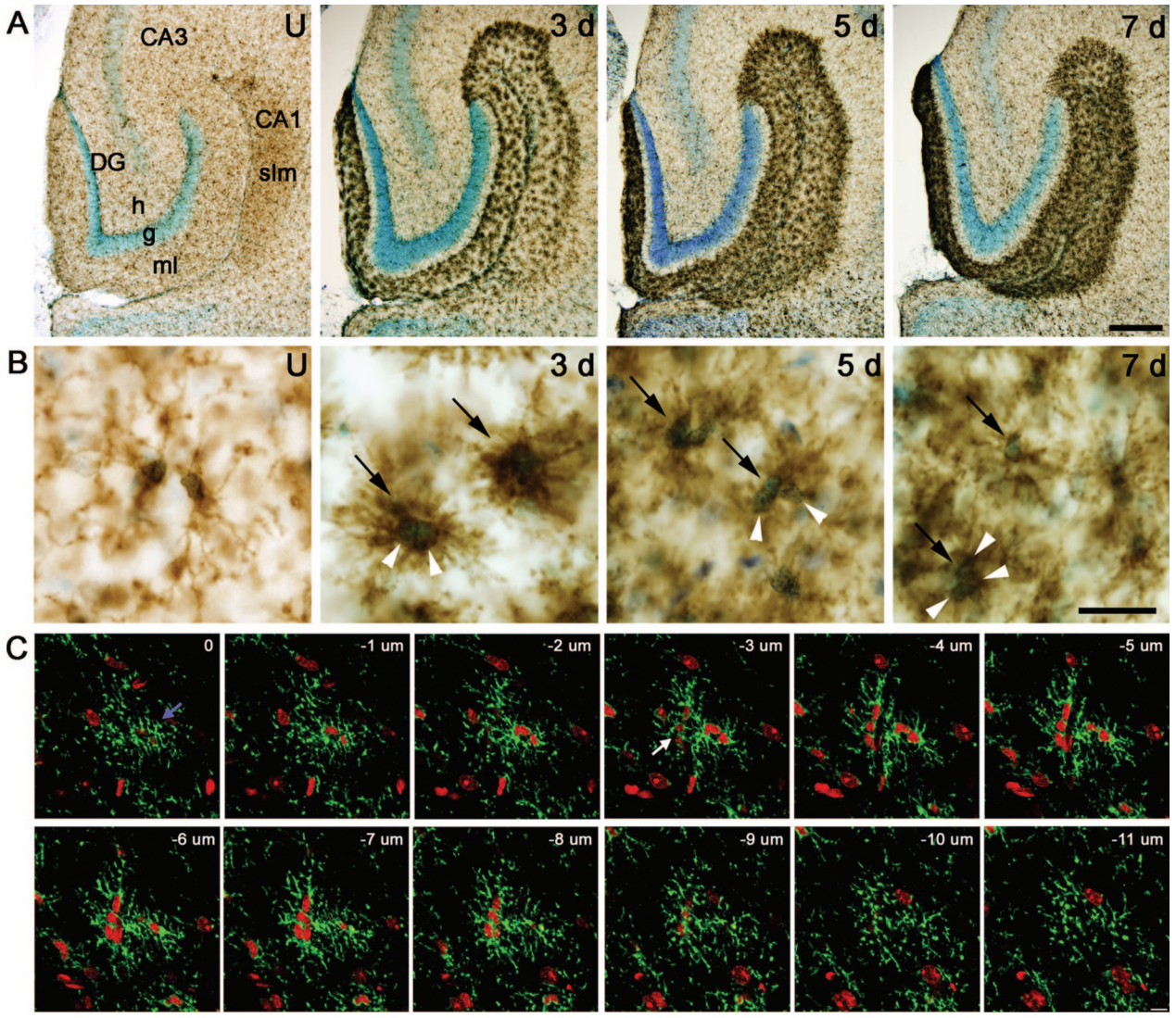

Figure 2. Time profile of reactive microgliosis in PP-deafferented dentate gyrus and hippocampus and cellular composition of reactive microglial clusters. **A:** Microglia are visualized in an unlesioned (U) mouse and 3, 5, and 7 days after PP transection by CD11b immunohistochemistry. **B:** High-power micrographs from the sections shown directly above in **A**. Three days after lesion, microglia in deafferented subregions have a dense hyperramified appearance, characteristic of activated cells, and many formed distinctly stained cellular clusters. Five and 7 days after lesion, the microglial reactivity is almost confluent, and it is difficult to clearly distinguish individual microglial cells and processes. **C:** Two multicellular microglial clusters are visualized in a series of 12 confocal microscopy images, 1 μm apart, 3 days after PP lesion. CD11b is visualized in green and propidium iodide-stained nuclei in red. An intraparenchymal microglial cluster containing two microglial cells (**blue arrow**) is present from 0 to -8 μm, and a juxtavascular microglial cluster containing three microglial cells (**white arrow**) is observed between -3 and -10 μm. Note also the green CD11b staining between individual nuclei. CA1, hippocampal CA1 region; CA3, hippocampal CA3 region; DG, dentate gyrus; g, granular cell layer; h, hilus; ml, molecular layer; slm, stratum lacunosum-moleculare; **black arrows**, clusters; **white arrowheads**, nuclei. Scale bars: 100 μm (**A**); 10 μm (**B**, **C**).

fewer macrophages were already observed by 7 days, which then comprised only ~0.5% of the CD11b$^+$ population.

Table 1. Estimates of Total CD11b$^+$ Microglial Cell Numbers

Animal	Day 3 *N* (CE)	Day 5 *N* (CE)	Day 7 *N* (CE)
1	24,300 (0.106)	26,000 (0.100)	17,300 (0.094)
2	23,100 (0.088)	25,100 (0.086)	25,900 (0.120)
3	22,200 (0.078)	21,900 (0.100)	25,500 (0.111)
4	20,200 (0.097)	16,300 (0.102)	26,900 (0.093)
5	23,600 (0.090)	22,900 (0.083)	24,700 (0.112)
Mean	22,700 (0.092)	22,400 (0.095)	24,100 (0.107)
SD	1600	3800	3900
CV	0.070	0.170	0.161

Microglial Proliferation after Axonal Lesion

The peak microglial proliferative response was observed 3 days after PP transection with 27% (11,000) BrdU$^+$ microglia in the deafferented hippocampus (Figure 4, A–C). Seven days after PP transection a lesion-induced

Table 2. Average Percentages of Different Cell Types Counted

Cell type	Day 3	Day 5	Day 7
Reactive microglia with one nucleus	5	5	2
Microglial clusters	76	72	75
Resting, ramified microglia	19	23	23

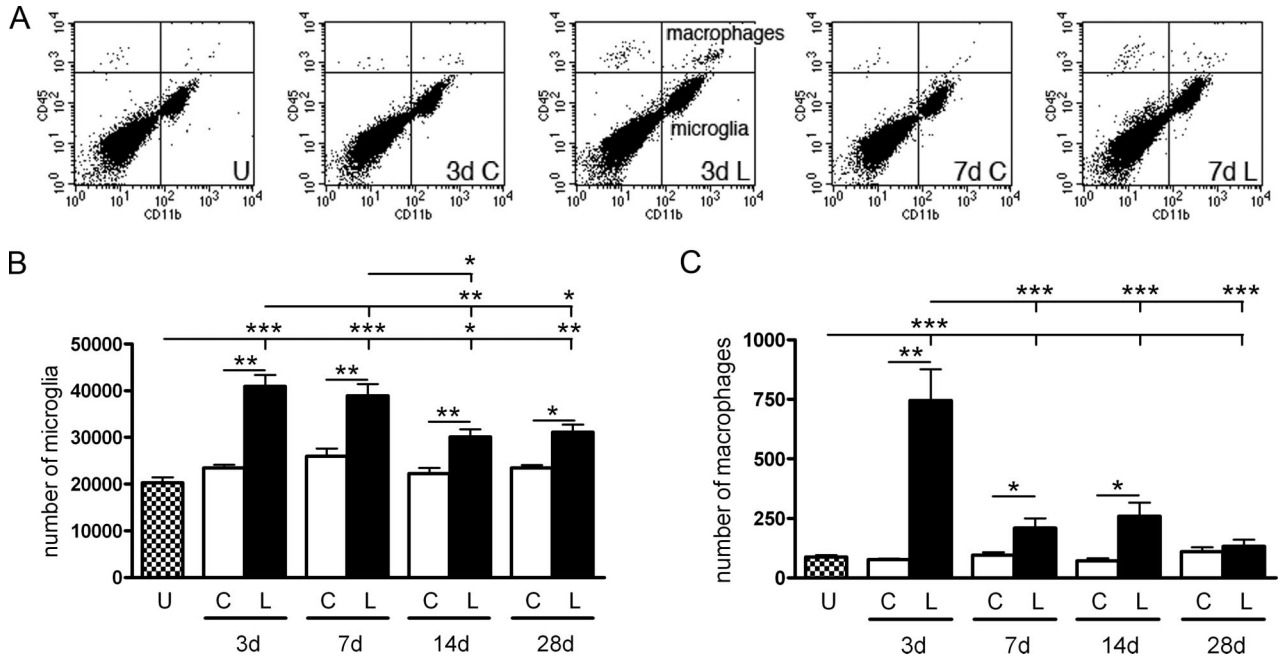

Figure 3. Microglia and macrophages in normal and deafferented hippocampus. **A:** Flow cytometry profiles, showing all viable (7-AAD-negative) cells in the forward/side scatter gated population, illustrate microglia ($CD45^{dim}CD11b^{+}$, bottom right quadrants) and macrophages ($CD45^{high}CD11b^{+}$, top right quadrants) in unmanipulated mice or 3 and 7 days after PP transection. Quantification of flow cytometry profiles reveals increases in both total numbers of microglia (**B**) and macrophages (**C**) in lesioned (L) hippocampi from C57BL/6 mice compared with contralateral (C) or unmanipulated (U) mice. Lesioned: 3 days ($n = 5$), 7 days ($n = 7$), 14 days ($n = 7$) and 28 days ($n = 6$). Unlesioned, $n = 6$. $^{*}P < 0.05$, $^{**}P < 0.01$, and $^{***}P < 0.001$.

microglial proliferative response was still present compared with the contralateral hippocampus when evaluated by the number of $BrdU^{+}$ microglia (Figure 4C). There was no statistically significant lesion-induced proliferative response in the macrophage population at any of the investigated times of observation evaluated by the percentage of $BrdU^{+}$ macrophages (Figure 4A, upper quadrants; and data not shown). This suggests that microglia proliferate readily in response to PP lesion, whereas macrophages rarely do. Because microglial clusters were prominent 3 days after lesion (Table 2), coinciding with microglial peak proliferation (Figure 4, A–C), it was investigated whether these clusters represented nests of proliferating microglia. PP-lesioned mice were pulse-labeled with BrdU 1 hour before perfusion, and the proliferation status of clustered tomato lectin^{+}

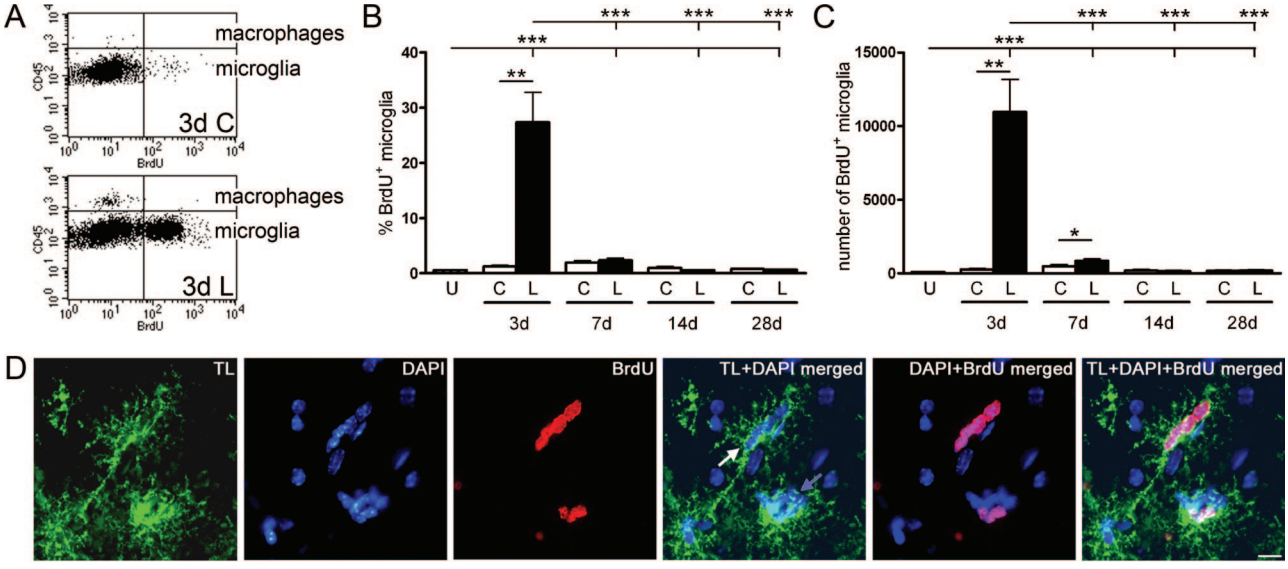

Figure 4. Microglial proliferation after PP lesion in C57BL/6 mice. **A:** Flow cytometry profiles, gated to show all $CD45^{+}CD11b^{+}$ cells, illustrate significant proliferation by $BrdU^{+}$ mitotic microglia (bottom quadrants) and little incorporation of BrdU by macrophages (top quadrants) 3 days after PP lesion. Quantification of the proportion (**B**) and number (**C**) of $BrdU^{+}$ microglia are displayed in bar graphs, after gating on $CD45^{dim}CD11b^{+}$ cells only. Microglial mitosis was visualized in histological sections using a combination of tomato lectin to identify microglia (green) and BrdU staining (red). **D:** As shown in the merged photograph, BrdU has been incorporated into several nuclei in both a juxtavascular cluster (**white arrow**) and an intraparenchymal cluster (**blue arrow**). $^{**}P < 0.01$, and $^{***}P < 0.001$. Scale bar = 10 μm.

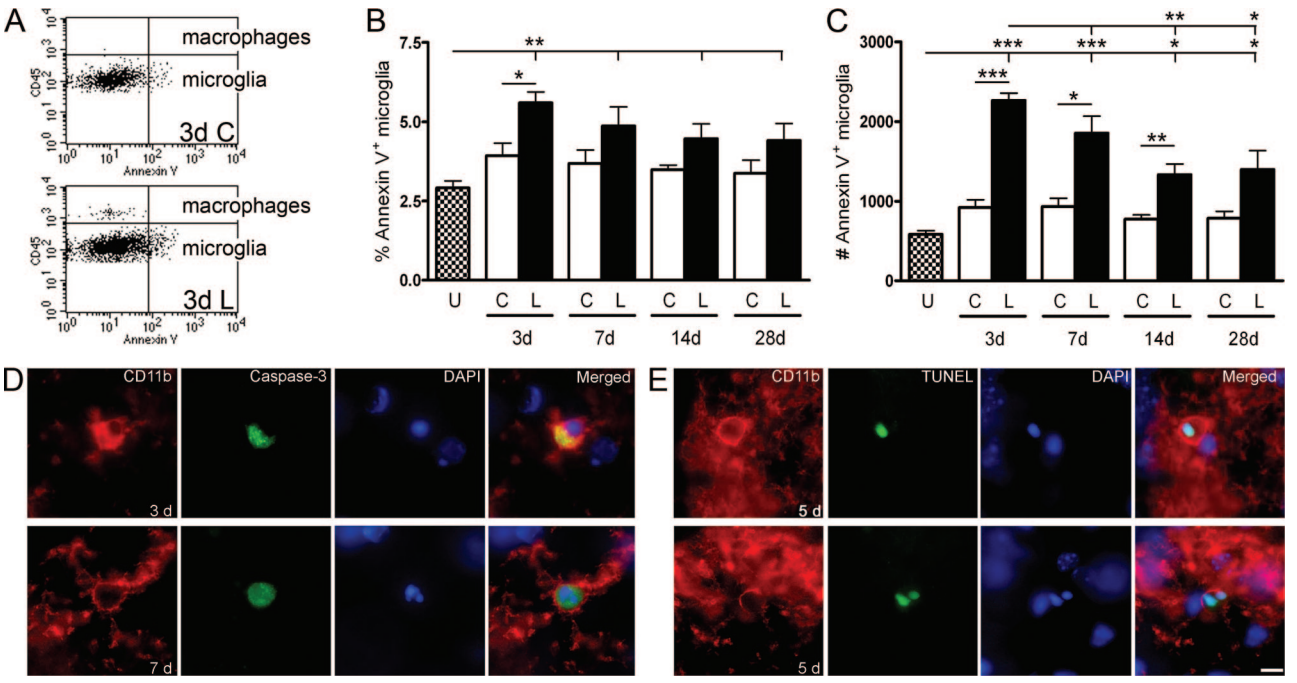

Figure 5. Microglial apoptosis after PP lesion in C57BL/6 mice. **A:** Flow cytometry profiles, gated to show all viable (7-AAD$^-$) CD45$^+$CD11b$^+$ cells, illustrate significant apoptosis by annexin V$^+$ microglia (bottom quadrants) and little apoptosis by macrophages (top quadrants), 3 days after PP lesion. Quantification of the proportion (**B**) and number (**C**) of annexin V$^+$ microglia are displayed in bar graphs, after gating specifically on CD45^{dim}CD11b$^+$ cells. **D:** Microglial apoptosis is visualized in PP deafferented dentate gyrus 3 and 7 days after lesion, using a combination of activated caspase-3 (green) and CD11b (red). Apoptotic CD11b$^+$ microglia labeled with TUNEL are shown 5 days after lesion. CD11b is shown red, and TUNEL in green. **E:** Note the nuclear fragmentation in the microglial cell shown in the bottom panel. $^*P < 0.05$, $^{**}P < 0.01$, and $^{***}P < 0.001$. Scale bar = 10 μm.

microglia was assessed by conventional fluorescence microscopy. BrdU incorporation was observed in some nuclei within the microglial clusters (Figure 4D).

Microglial Apoptosis after Axonal Lesion

The apoptotic response was investigated using annexin V as marker for apoptosis (Figure 5, A–C). Annexin V binds to phosphatidylserine exposed in the outer leaflet of the plasma membrane of apoptotic cells, and hence only works in intact cells because phosphatidylserine is normally present in the inner leaflet of the plasma membrane. Dead cells were excluded from the flow cytometric analysis by applying the viability marker 7-AAD. A lesion-induced apoptotic response was observed 3, 7, and 14 days after PP transection and was reflected in an increase in the total number of annexin V$^+$ microglia (Figure 5C). At 28 days, numbers of annexin V$^+$ microglia were significantly elevated versus unlesioned hippocampi, but not compared with the contralateral hippocampus. However, because of the changing number of microglia a lesion-induced increase in the proportion of apoptotic annexin V$^+$ microglia was only observed 3 days after lesion (Figure 5B). In the macrophage population a lesion-induced apoptotic response was only observed in the number of annexin V$^+$ macrophages 14 days after lesion compared with the contralateral hippocampus but not versus unlesioned hippocampi (Figure 5A, upper quadrants at 3 days; and data not shown).

Based on observations of activated caspase-3$^+$ process-bearing cells in deafferented hippocampal regions in PP-lesioned mice 3, 5, and 7 days after lesion (n = 2 to 3 per group), apoptotic microglia were visualized in the molecular layer of the dentate gyrus 3, 5, and 7 days after PP lesion. Activated caspase-3 was present throughout the cytoplasm of CD11b$^+$ microglia (Figure 5D). A void in the staining was apparent where the condensed DAPI-stained nuclear remains were situated. Plasma membrane blebbing and cell rounding was apparent (Figure 5D), both phenomena occurring as the cytoskeletal proteins are broken down by activated caspases.[36] Microglial DNA fragmentation as an indication of apoptosis in the molecular layer was also visualized using TUNEL and co-labeling with CD11b in the deafferented molecular layer 5 days after lesion (Figure 5E). The DNA fragmentation was clearly visualized by the dUTP labeling of the condensed nucleus, which overlapped with the DAPI DNA staining. These microglia also displayed the plasma membrane blebbing and cell rounding characteristic of apoptotic cells (Figure 5E). Taken together, the data therefore suggest that occurring in parallel with the lesion-induced reactive proliferation of microglia is microglial cell death by apoptosis.

Increases in Macrophage Colony-Stimulating Factor (M-CSF) and M-CSFR mRNA Levels Coincide with Elevations in CD11b mRNA

M-CSF and its receptor, M-CSFR, have been shown to be essential for microglial proliferation in other neural lesion models.[37,38] Granulocyte-macrophage colony stimulat-

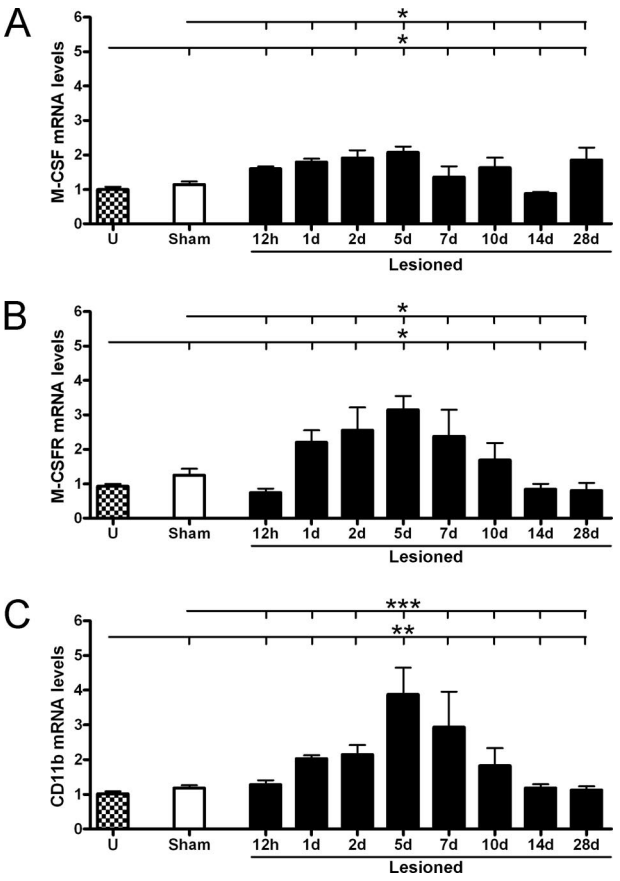

Figure 6. Increased mRNA levels of M-CSF and M-CSFR coincide with maximal CD11b expression. Levels of M-CSF (**A**), M-CSFR (**B**), and CD11b (**C**) mRNA were measured by real-time PCR in hippocampal samples from unmanipulated (U), sham-operated, or lesioned C57BL/6 mice between 12 hours and 28 days after lesion. Data were normalized with HPRT1. $^{*}P < 0.05$, $^{**}P < 0.01$, and $^{***}P < 0.001$.

ing factor (GM-CSF) signaling via the GM-CSF receptor (GM-CSFR) has also been implicated in microglial proliferation.[39,40] Changes in levels of M/GM-CSF and M/GM-CSFR mRNA as well as CD11b mRNA were therefore investigated at different intervals from 12 hours to 28 days after lesion (Figure 6). Levels of M-CSF and M-CSFR mRNA levels were significantly elevated at 5 days (Figure 6, A and B), which coincided with the time of maximal microglial expression of CD11b mRNA (Figure 6C). GM-CSF mRNA was only detected at very low levels in unmanipulated and deafferented hippocampi, with real-time PCR cycle thresholds ≥38. No significant changes in mRNA levels of GM-CSF/GM-CSFR were observed (data not shown). Preliminary screenings did not reveal any changes in mRNA levels at 3 or 6 hours either (data not shown).

Lesion-Induced Immigration of BM Cells

Based on previous observations that BM-derived cells contribute to reactive microgliosis in PP-lesioned mice,[11] it was investigated whether proliferative and apoptotic mechanisms of population control applied equally to resident and immigrant microglial cells using GFP BM chimeric mice (Figure 7A). A lesion-induced increase in the proportion of immigrating GFP^+ microglia was observed 7 days after PP lesion (Figure 7B). At this time, ~5% of $CD45^{dim}CD11b^+$ cells expressed GFP. Significant lesion-induced immigration of $GFP^+CD45^{dim}CD11b^+$ microglia was not observed at 3 or 5 days. As expected, 70 to 75% of $CD45^{high}CD11b^+$ macrophages detected after PP lesion were GFP^+ (data not shown). To verify the integration of the BM-derived cells into the neural parenchyma, BM chimeras were analyzed histologically ($n = 4$), 7 days after lesion. Immigrating GFP^+ BM-derived microglia specifically infiltrated the deafferented areas of the dentate gyrus, CA3 and CA1 (Figure 7C, shown for the dentate gyrus), as previously shown in other types of BM chimeric mice.[34,41]

Impaired Microglial Responses in BM Chimeric Mice

Having observed a significant increase in the number of microglia in the PP-deafferented hippocampus 3 days after lesion, we anticipated a similar increase in BM chimeric mice. Surprisingly, the lesion-induced increase in microglial numbers was absent in BM chimeric mice 3 days after lesion (Figure 8A). Microglial numbers were significantly elevated compared with the contralateral hippocampus 5 and 7 days after lesion. Microglial responses to PP lesion in chimeric and C57BL/6 mice 3 days after PP lesion were therefore compared. Included in this analysis was a group of B6(CD45.1) mice because these congenic mice were used as BM transplant recipients. As expected, a significant increase in the number of microglia was observed in the PP-deafferented hippocampus compared with contralateral hippocampus in C57BL/6 and B6(CD45.1) mice (1.6- and 1.9-fold, respectively; Figure 8A). In doing this comparison, it also became evident that the estimated total number of microglia in the contralateral hippocampi in the BM chimeric mice was significantly smaller compared with C57BL/6 and B6(CD45.1) mice (Figure 8A).

Microglial mitotic activity was then assessed because mice used in flow cytometric analyses had been injected with BrdU three times throughout the past 24 hours before perfusion. In accordance with the observed differences in microglial numbers, the number of proliferating $BrdU^+$ microglia in the PP-deafferented hippocampus in C57BL/6 mice was 11,300 and 14,800 in B6(CD45.1) mice. Both were significantly higher than the 600 $BrdU^+$ microglia observed in the BM chimeras (Figure 8B). In all groups of mice, numbers and proportions of proliferating microglia in the deafferented hippocampi were significantly higher compared with contralateral hippocampi (Figure 8B). Whereas low proportions of microglia were proliferating in the contralateral hippocampus of C57BL/6, B6(CD45.1) and chimeric mice (4, 2, and 2%, respectively), the proportion of $BrdU^+$ microglia was 6% in deafferented hippocampi of chimeric mice compared with the significantly higher 34% in C57BL/6 mice and 33% in B6(CD45.1) mice. In chimeric mice, numbers and proportions of proliferating $BrdU^+$ microglia remained

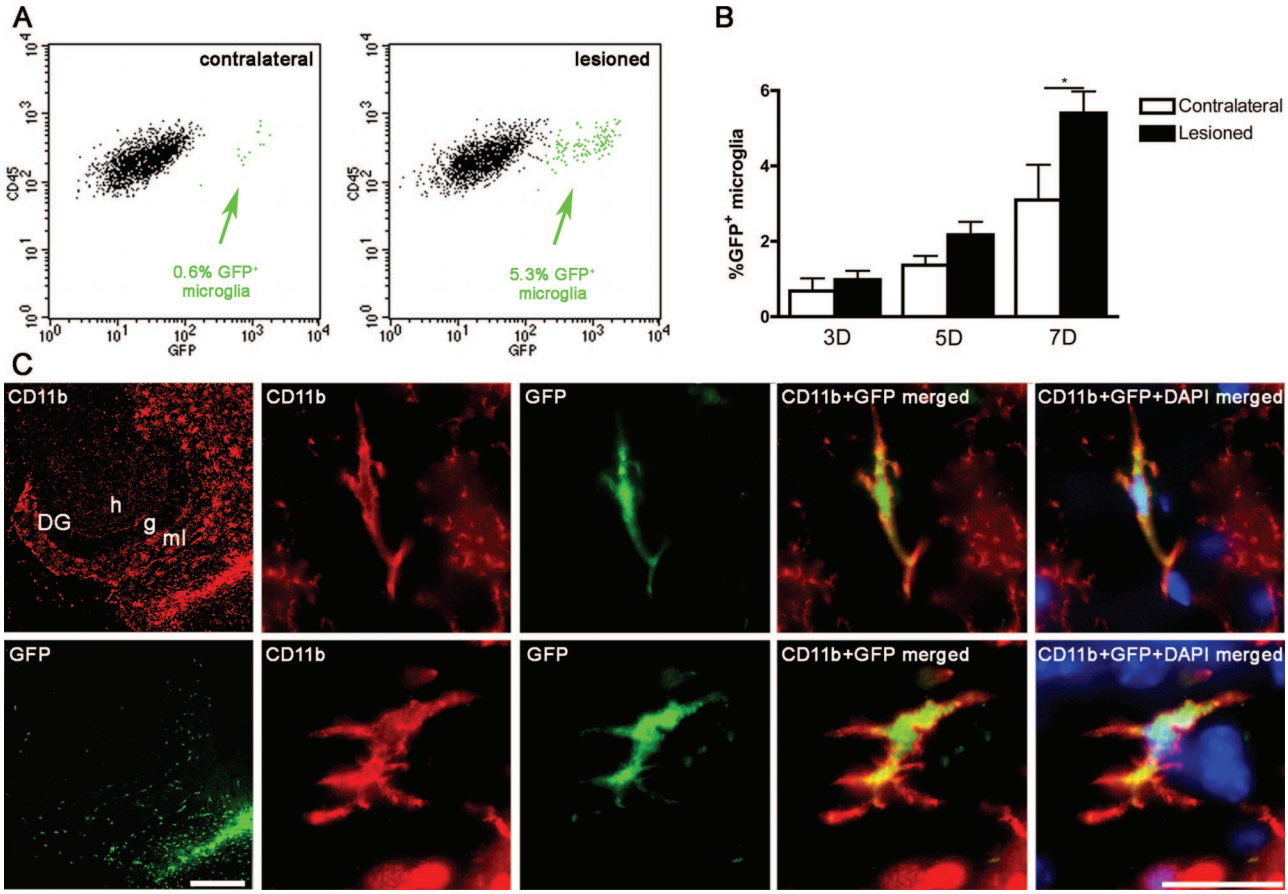

Figure 7. Immigrant BM-derived GFP^+ microglia infiltrate the PP deafferented hippocampus. Microglia were defined as $CD45^{dim}CD11b^+$ in flow cytometry and the percentage of immigrant GFP^+ microglia was analyzed in contralateral and lesioned hippocampi. **A: Arrows** indicate the percentages of GFP^+ microglia in the contralateral and lesioned samples. **B:** Percentages of $GFP^+CD45^{dim}CD11b^+$ microglia in contralateral and lesioned hippocampi. **C:** Micrographs showing lesion-specific infiltration of immigrant GFP^+ microglia visualized by the expression of green GFP fluorescence and labeled by CD11b immunohistochemistry in red. DG, dentate gyrus; g, granular cell layer; h, hilus; ml, molecular layer. Scale bars: 200 μm (**C**, left); 20 μm (**C**, right).*$P < 0.05$.

significantly elevated at 5 and 7 days after lesion (Figure 8B and data not shown). Observed increases in mitotic microglial numbers were lesion-induced because numbers were significantly smaller in contralateral hippocampi (Figure 8B).

Microglial apoptotic responses were also investigated in the chimeric mice, using annexin V as marker for apoptosis (Figure 8C). As before, dead cells were excluded from the analysis by applying the viability marker 7-AAD. No statistically significant differences were observed in numbers of apoptotic microglia at 3 or 5 days after lesion, although a lesion-induced increase in the proportion of apoptotic microglia was observed after 3 days. By 7 days, both the number and proportion of annexin V^+ microglia were significantly increased (Figure 8C and data not shown). Numbers of apoptotic microglia were significantly lower in chimeric mice than in C57BL/6 or B6(CD45.1) mice (Figure 8C), although the relative proportions of annexin V^+ microglia in deafferented hippocampi were not significantly different between groups (5.2% versus 5.6% and 6.8%, respectively). Microglial mitotic and apoptotic responses were comparable in C57BL/6 and congenic B6(CD45.1) mice 3 days after lesion, although the total number of microglia was slightly higher in B6(CD45.1) mice.

Mitotic and Apoptotic Responses in Microglial Populations in BM Chimeric Mice

The contribution of immigrant GFP^+ and resident GFP^- microglia to the proliferative response after lesion was subsequently analyzed (Figure 9A). Mitotic expansion of the microglial population predominantly took place among the resident GFP^- microglia (Figure 9B). The estimated number of proliferating immigrant GFP^+ microglia was small but increased significantly during the later phase of the microglial reaction 7 days after lesion (Figure 9C). Overall, the observation of steadily increasing microglial numbers (Figure 8A), and the almost constant numbers of $BrdU^+$ and GFP^-BrdU^+ microglia observed in the same mice (Figure 9, B and C), was reflected in a decreasing proportion of all microglia and resident GFP^- microglia undergoing proliferation during the period of observation. Whereas 6% of resident GFP^- microglia proliferated 3 days after lesion, this proportion was significantly reduced to 3% 7 days after lesion. By contrast, a significantly larger proportion of GFP^+BrdU^+ immigrant microglia were induced to proliferate at 7 days after lesion (0.20%) than 3 days after lesion (0.04%).

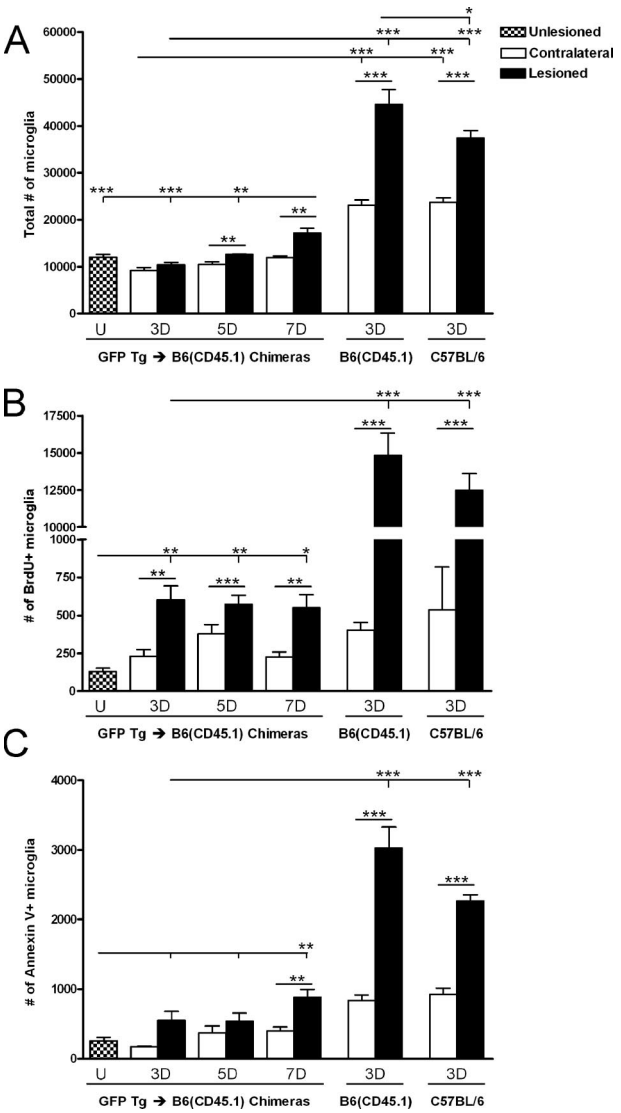

Figure 8. Microglial expansion and responses are impaired after PP lesion in BM chimeric mice. **A:** Estimates of the total number of $CD45^{dim}CD11b^{+}$ microglia in BM chimeric mice showed no increase after axonal lesion until 5 to 7 days in lesioned hippocampi over contralateral or unlesioned hippocampi, unlike in C57BL/6 and congenic B6(CD45.1) mice, which showed significant increases by 3 days. **B:** Microglial mitotic activity was also impaired in BM chimeric versus C57BL/6 and B6(CD45.1) mice at 3 days. **C:** The number of annexin V^{+} microglia was similarly reduced in BM chimeric mice. $^{*}P < 0.05$, $^{**}P < 0.01$, and $^{***}P < 0.001$.

Finally, when analyzing apoptotic resident GFP^{-} and immigrating GFP^{+} microglia independently there was no statistically significant lesion-induced apoptosis 3 or 5 days after lesion in either population by numbers (Figure 9, D–F) or proportions (data not shown). Seven days after PP deafferentation, however, a statistically significant lesion-induced apoptotic response was evident in both the resident GFP^{-} and the immigrant GFP^{+} microglial populations (Figure 9, E and F). However, the proportion of apoptotic GFP^{-} resident microglia were similar in deafferented (4%) and contralateral (3%) hippocampus. In comparison, in the immigrant GFP^{+} microglial population there was an increase in apoptotic cells from 0.32% in contralateral hippocampi to 0.71% in deafferented hippocampi.

Discussion

This study aimed to investigate the cellular population control of resident and immigrant microglia by combining the use of BM chimeric mice and a classic model for axonal lesion-induced reactive microgliosis in the dentate gyrus and hippocampus. The present work demonstrates that the lesion-induced increase in microglial numbers from 3 to 7 days after PP transection is balanced by simultaneously occurring mitosis and apoptosis but also that microglial numbers remain elevated for weeks after the injury. In the BM chimeric mice, the resident microglial population displayed a lesion-induced mitotic response, whereas a comparable lesion-induced apoptotic response was observed in resident and immigrant microglia. The present work also demonstrates the microglial population and the lesion-induced mitotic activity of resident microglia to be severely reduced in BM chimeric mice.

BM chimeric mice have been used extensively for studies of microglial turnover and replacement[42,43] and in studies focusing on the possibility of using BM-derived cells for gene therapy.[10,44] However, the model has the disadvantage of whole-body irradiation of the host to eradicate host BM cells before transplantation, which could potentially induce microglial activation or cell death. The reduction of the microglial population in the BM chimeras to 30% of that observed in the normal mice after PP lesion was unexpected, as was the observation that the mitotic activity of microglia in BM chimeras was severely impaired. Still, a significant but delayed lesion-induced increase in mitosis of resident microglia accounted for almost all of the mitosis observed.

Measuring apoptosis in cells obtained from tissue using flow cytometry is difficult because the relatively extended period of time cells are processed *ex vivo* and the processing itself could potentially increase the number of apoptotic cells. This, however, was partly compensated for because the contralateral and deafferented hippocampi from the same animal were processed concurrently. In this way, any difference between the deafferented hippocampus and the contralateral hippocampus would be attributable to reactive microgliosis, although the actual percentage of apoptotic microglia measured could be artificially high. Annexin V binding is a sensitive marker for apoptosis but has also been demonstrated to bind to viable B cells at intermediate levels and can therefore not be regarded as a marker only for apoptosis. Dead or dying cells, however, express higher levels of annexin V binding.[45] Apoptotic annexin V^{+} cells are therefore only to be gated as cells expressing the highest levels of annexin V for the purpose of excluding any potentially false-positive cells.

Stereology is a quantitative method available for obtaining an unbiased estimate of the number of cells in three-dimensional structures in histological sections, and it is unaffected by deafferentation-induced shrinkage and

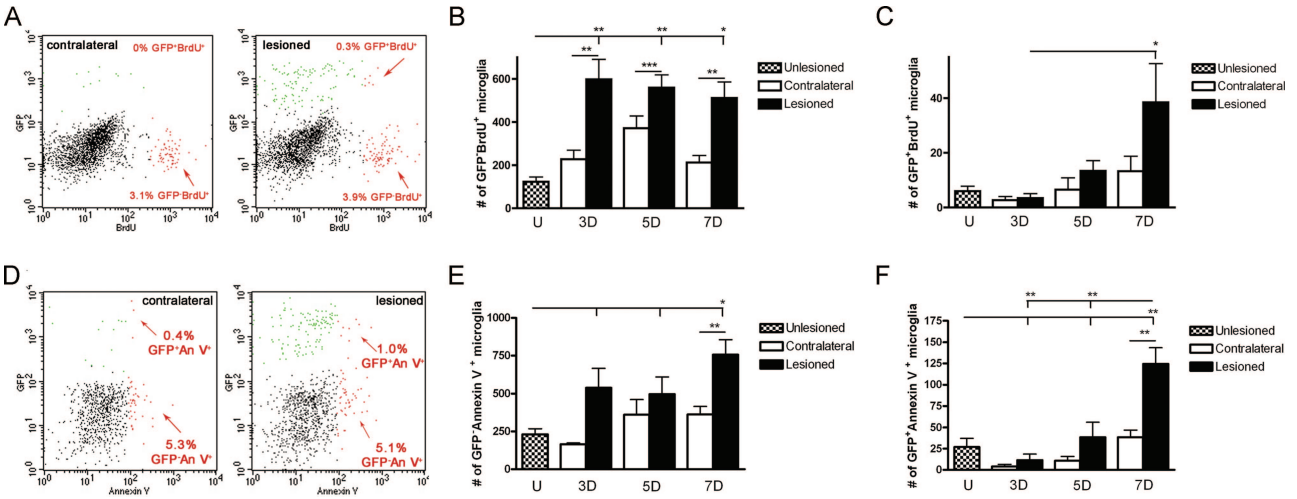

Figure 9. Mitotic activity and apoptotic response of immigrant and resident microglia in PP-deafferented hippocampus in BM chimeric mice. **A:** Flow cytometry dot plots gated on $CD45^{dim}CD11b^{+}$ microglia illustrating $BrdU^{+}$ mitotic immigrant GFP^{+} and resident GFP^{-} microglia (**arrows**) 7 days after PP lesion. **B** and **C:** Total numbers of $GFP^{-}BrdU^{+}$ resident and $GFP^{+}BrdU^{+}$ immigrant microglia in the PP-deafferented hippocampus. **D:** Flow cytometry dot plots gated on $CD45^{dim}7\text{-}AAD^{-}$ microglia illustrating annexin V^{+} apoptotic immigrant GFP^{+} and resident GFP^{-} microglia, 7 days after PP lesion. **E** and **F:** Numbers of GFP^{-} annexin V^{+} and GFP^{+} annexin V^{+} $CD45^{dim}7\text{-}AAD^{-}$ microglia in the PP-deafferented hippocampus, respectively. $^{*}P < 0.05$, $^{**}P < 0.01$, and $^{***}P < 0.001$.

deformation of the dentate gyrus.[46,47] Therefore, it was the method of choice for answering the question of global changes in microglial cell numbers. The limited resolution of the light microscope in the immunohistochemically stained thick tissue sections, however, proved to be a limitation to the level of cellular detail that could be obtained. To make up for the loss of cellular resolution, it was taken into consideration that reactive microglia during the stereological and confocal analysis often were observed to occur in multicellular microglial clusters. As earlier mentioned, the actual number of microglia would therefore be at least twofold and possibly threefold higher, as also calculated in studies based on density estimations.[14,34] This would also be in accordance with the observation of an approximately fourfold up-regulation of CD11b mRNA levels in PP-deafferented isolated hippocampi 5 days after lesion.

Unexpectedly, flow cytometry might be superior to answer questions about changes in total microglial cell numbers because the dissociation procedure makes all microglia accessible to analysis. A disadvantage was that nonaffected areas were also included in the analysis, and that there is inevitably cell loss during the preparation procedure. Still, a 74% increase in microglial cell numbers was detected in deafferented compared with contralateral hippocampus 3 days after lesion in C57BL/6 mice. Flow cytometry also proved its strength in the functional analyses of mitotic and apoptotic responses in microglial subpopulations, because of the high rate at which multiple parameters could be acquired on a single cell basis, which enabled investigation of small subpopulations. Analysis of rare events such as $BrdU^{+}$ and annexin V^{+} cells in the immigrating GFP^{+} population of microglia could introduce uncertainties, but again, comparing the deafferented hippocampus with the contralateral offers a good internal control. Parenchymal microglia express lower levels of CD45 ($CD45^{dim}$) compared with leukocytes ($CD45^{high}$). Perivascular cells are known to readily turn over with blood cells[48] and it cannot be excluded that some perivascular cells might fall into the $CD45^{dim}$ gate in flow cytometric analysis.

Because the phenomenon of lesion-induced enhanced immigration of BM-derived microglia became generally accepted[10] an increasing number of studies have been published on the subject.[11,42,43] The phenomenon of BM-derived cells homing to areas of brain damage and reactive microgliosis opens the perspective of using a naturally occurring event to target cells engineered for a specific purpose into a pathological area of the CNS, an approach demonstrated to be plausible.[12,13] For a therapeutic technique like this to be safe and applicable for possible use in humans, the population control of such immigrating BM-derived cells would have to be efficient to avoid induction of malignancies or widespread necrosis in these areas of infiltrating cells. Microglial mitosis is an essential part of microglial turnover[9] and reactive microgliosis.[49,50] Mitosis, in combination with recruitment of immigrating BM-derived cells and migration of microglia from adjoining areas, expands the microglial population.[10,15] Throughout the period studied here, it was not possible to show a statistically significant increase in mitosis by immigrant GFP^{+} microglia until day 7, which was in contrast to the significant mitotic response in the resident microglial population at both 3, 5, and 7 days. Although, this indicates that these cells constitute a controlled supplement to the microglial population, studies of immigrant cell proliferation in BM chimeric mice with longer survival times should be performed to determine whether BM-derived microglia pose a threat of unrestricted mitosis.

Microglia are known to be susceptible to apoptosis as described *in vitro*[16] and in the model of experimental autoimmune encephalomyelitis.[51] Apoptosis has been suggested as an important mode of microglial population control, however, through a nonclassic pathway that does not culminate with condensed fragmented DNA.[16]

The present study has demonstrated that apoptosis does play a role in control of the microglial population in brain regions displaying a dense anterograde axonal and terminal degeneration in both resident and immigrating microglia as investigated by identification of phosphatidylserine externalization by annexin V binding. Furthermore, it was shown that microglia indeed can undergo apoptosis in a classic sense with apoptotic morphology, condensed fragmented DNA, and cytoplasmic expression of activated caspase-3. This does point toward immigrating microglia being governed by a similar mechanism of cellular clearance by apoptosis as resident microglia.

At present, the key molecules and signaling pathways involved in microglial mitosis and apoptosis in the deafferented dentate gyrus are unknown, but likely candidates are macrophage colony-stimulating factor (M-CSF) and granulocyte macrophage colony-stimulating factor (GM-CSF).[37,38,40] After peripheral axotomy, microglia in the facial motor nucleus increase their expression of M-CSF receptors and increase their binding of M-CSF and GM-CSF before or at the onset of microglial proliferation.[39,52] Although the presently observed up-regulation of M-CSF and M-CSF receptor mRNA levels 5 days after lesion occurs relatively late compared with the peak microglial proliferation 3 days after lesion, it should be taken into consideration that changes in mRNA levels were determined based on analysis of whole hippocampi, not allowing direct assessment of up-regulation of these molecules or the GM-CSF and GM-CSF receptor in the areas of microglial mitosis. M-CSF also plays an essential role in the maintenance of the microglial cell population in the normal adult CNS,[38] which is in line with studies of cultured microglia showing that deprivation of M-CSF results in microglial apoptosis.[53] Overall, this study broadens our understanding of microglial response to neural lesion by showing that simultaneously occurring mitosis and apoptosis regulate expansion and reduction of resident as well as immigrant microglial populations after acute neural damage.

Acknowledgments

We thank Christina Fenger, Mads D. Pedersen, and Lene Sylvest for assistance with experiments; Lene Jørgensen and Sussanne Petersen for technical assistance; and Werner Vach for statistical counseling.

References

1. Kreutzberg GW: Microglia: a sensor for pathological events in the CNS. Trends Neurosci 1996, 19:312–318
2. Nimmerjahn A, Kirchhoff F, Helmchen F: Resting microglial cells are highly dynamic surveillants of brain parenchyma in vivo. Science 2005, 308:1314–1318
3. Davalos D, Grutzendler J, Yang G, Kim JV, Zuo Y, Jung S, Littman DR, Dustin ML, Gan WB: ATP mediates rapid microglial response to local brain injury in vivo. Nat Neurosci 2005, 8:752–758
4. Streit WJ, Walter SA, Pennell NA: Reactive microgliosis. Prog Neurobiol 1999, 57:563–581
5. Aloisi F: Immune function of microglia. Glia 2001, 36:165–179
6. Takahashi K, Rochford CDP, Neumann H: Clearance of apoptotic neurons without inflammation by microglial triggering receptor expressed on myeloid cells-2. J Exp Med 2005, 201:647–657
7. Paloneva J, Kestila M, Wu J, Salminen A, Bohling T, Ruotsalainen V, Hakola P, Bakker ABH, Phillips JH, Pekkarinen P, Lanier LL, Timonen T, Peltonen L: Loss of function mutations in TYROBP (DAP12) result in a presenile dementia with bone cysts. Nat Genet 2000, 25:357–361
8. del Rio-Hortega P: Microglia. Cytology and Cellular Pathology of the Nervous System. Edited by W Penfield. New York, Paul B. Hoeber, 1932, pp 481–534
9. Lawson LJ, Perry VH, Gordon S: Turnover of resident microglia in the normal adult-mouse brain. Neuroscience 1992, 48:405–415
10. Priller J, Flugel A, Wehner T, Boentert M, Haas CA, Prinz M, Fernandez-Klett F, Prass K, Bechmann I, de Boer BA, Frotscher M, Kreutzberg GW, Persons DA, Dirnagl U: Targeting gene-modified hematopoietic cells to the central nervous system: use of green fluorescent protein uncovers microglial engraftment. Nat Med 2001, 7:1356–1361
11. Wirenfeldt M, Babcock AA, Ladeby R, Lambertsen KL, Dagnaes-Hansen F, Leslie RG, Owens T, Finsen B: Reactive microgliosis engages distinct responses by microglial subpopulations after minor central nervous system injury. J Neurosci Res 2005, 82:507–514
12. Biffi A, De Palma M, Quattrini A, Del Carro U, Amadio S, Visigalli I, Sessa M, Fasano S, Brambilla R, Marchesini S, Bordignon C, Naldini L: Correction of metachromatic leukodystrophy in the mouse model by transplantation of genetically modified hematopoietic stem cells. J Clin Invest 2004, 113:1118–1129
13. Asheuer M, Pflumio FO, Benhamida S, Dubart-Kupperschmitt A, Fouquet F, Imai Y, Aubourg P, Cartier N: Human CD34(+) cells differentiate into microglia and express recombinant therapeutic protein. Proc Natl Acad Sci USA 2004, 101:3557–3562
14. Hailer NP, Grampp A, Nitsch R: Proliferation of microglia and astrocytes in the dentate gyrus following entorhinal cortex lesion: a quantitative bromodeoxyuridine-labelling study. Eur J Neurosci 1999, 11:3359–3364
15. Rappert A, Bechmann I, Pivneva T, Mahlo J, Biber K, Nolte C, Kovac AD, Gerard C, Boddeke HWGM, Nitsch R, Kettenmann H: CXCR3-dependent microglial recruitment is essential for dendrite loss after brain lesion. J Neurosci 2004, 24:8500–8509
16. Jones LL, Banati RB, Graeber MB, Bonfanti L, Raivich G, Kreutzberg GW: Population control of microglia: does apoptosis play a role? J Neurocytol 1997, 26:755–770
17. Schaefer BC, Schaefer ML, Kappler JW, Marrack P, Kedl RM: Observation of antigen-dependent $CD8^+$ T-cell/dendritic cell interactions in vivo. Cell Immunol 2001, 214:110–122
18. Hjorth-Simonsen A: Projection of the lateral part of the entorhinal area to the hippocampus and fascia dentata. J Comp Neurol 1972, 146:219–232
19. Fifková E: Two types of terminal degeneration in molecular layer of dentate fascia following lesions of entorhinal cortex. Brain Res 1975, 96:169–175
20. Matthews DA, Cotman C, Lynch G: Electron-microscopic study of lesion-induced synaptogenesis in dentate gyrus of adult rat. 1. Magnitude and time course of degeneration. Brain Res 1976, 115:1–21
21. Amaral DG, Witter MP: Hippocampal formation. The Rat Nervous System. San Diego, Academic Press, Inc., 1995, pp 443–493
22. Babcock AA, Kuziel WA, Rivest S, Owens T: Chemokine expression by glial cells directs leukocytes to sites of axonal injury in the CNS. J Neurosci 2003, 23:7922–7930
23. Meldgaard M, Fenger C, Lambertsen KL, Pedersen MD, Ladeby R, Finsen B: Validation of two reference genes for mRNA level studies of murine disease models in neurobiology. J Neurosci Methods 2006, 156:101–110
24. Babcock AA, Wirenfeldt M, Holm T, Nielsen HH, Dissing-Olesen L, Toft-Hansen H, Millward JM, Landmann R, Rivest S, Finsen B, Owens T: Toll-like receptor 2 signaling in response to brain injury: an innate bridge to neuroinflammation. J Neurosci 2006, 26:12826–12837
25. Ford AL, Goodsall AL, Hickey WF, Sedgwick JD: Normal adult ramified microglia separated from other central-nervous-system macrophages by flow cytometric sorting. Phenotypic differences defined and direct ex-vivo antigen presentation to myelin basic protein-reactive Cd4(+) T-cells compared. J Immunol 1995, 154:4309–4321
26. Sedgwick JD, Schwender S, Imrich H, Dorries R, Butcher GW, Termeulen V: Isolation and direct characterization of resident microglial

cells from the normal and inflamed central nervous system. Proc Natl Acad Sci USA 1991, 88:7438–7442
27. Renno T, Krakowski M, Piccirillo C, Lin JY, Owens T: TNF-α expression by resident microglia and infiltrating leukocytes in the central nervous system of mice with experimental allergic encephalomyelitis. Regulation by Th1 cytokines. J Immunol 1995, 154:944–953
28. West MJ, Slomianka L, Gundersen HJG: Unbiased stereological estimation of the total number of neurons in the subdivisions of the rat hippocampus using the optical fractionator. Anat Rec 1991, 231:482–497
29. Wirenfeldt M, Dalmau I, Finsen B: Estimation of absolute microglial cell numbers in mouse fascia dentata using unbiased and efficient stereological cell counting principles. Glia 2003, 44:129–139
30. Fagan AM, Gage FH: Cholinergic sprouting in the hippocampus: a proposed role for IL-1. Exp Neurol 1990, 110:105–120
31. Fagan AM, Gage FH: Mechanisms of sprouting in the adult central-nervous-system—cellular-responses in areas of terminal degeneration and reinnervation in the rat hippocampus. Neuroscience 1994, 58:705–725
32. Jensen MB, Gonzalez B, Castellano B, Zimmer J: Microglial and astroglial reactions to anterograde axonal degeneration: a histochemical and immunocytochemical study of the adult-rat fascia-dentata after entorhinal perforant path lesions. Exp Brain Res 1994, 98:245–260
33. Hjorth-Simonsen A, Jeune B: Origin and termination of hippocampal perforant path in rat studied by silver impregnation. J Comp Neurol 1972, 144:215–232
34. Ladeby R, Wirenfeldt M, Dalmau I, Gregersen R, Garcia-Ovejero D, Babcock A, Owens T, Finsen B: Proliferating resident microglia express the stem cell antigen CD34 in response to acute neural injury. Glia 2005, 50:121–131
35. Long JM, Kalehua AN, Muth NJ, Hengemihle JM, Jucker M, Calhoun ME, Ingram DK, Mouton PR: Stereological estimation of total microglia number in mouse hippocampus. Proc Natl Acad Sci USA 1998, 84:101–108
36. Kothakota S, Azuma T, Reinhard C, Klippel A, Tang J, Chu KT, McGarry TJ, Kirschner MW, Koths K, Kwiatkowski DJ, Williams LT: Caspase-3-generated fragment of gelsolin: effector of morphological change in apoptosis. Science 1997, 278:294–298
37. Raivich G, Morenoflores MT, Moller JC, Kreutzberg GW: Inhibition of posttraumatic microglial proliferation in a genetic model of macrophage-colony-stimulating factor deficiency in the mouse. Eur J Neurosci 1994, 6:1615–1618
38. Rogove AD, Lu W, Tsirka SE: Microglial activation and recruitment, but not proliferation, suffice to mediate neurodegeneration. Cell Death Differ 2002, 9:801–806
39. Raivich G, Gehrmann J, Kreutzberg GW: Increase of macrophage colony-stimulating factor and granulocyte-macrophage colony-stimulating factor receptors in the regenerating rat facial nucleus. J Neurosci Res 1991, 30:682–686
40. Suh HS, Kim MO, Lee SC: Inhibition of granulocyte-macrophage colony-stimulating factor signaling and microglial proliferation by anti-CD45RO: role of Hck tyrosine kinase and phosphatidylinositol 3-kinase/Akt. J Immunol 2005, 174:2712–2719
41. Bechmann I, Goldmann J, Kovac AD, Kwidzinski E, Simburger E, Naftolin F, Dirnagl U, Nitsch R, Priller J: Circulating monocytic cells infiltrate layers of anterograde axonal degeneration where they transform into microglia. FASEB J 2005, 19:647–649
42. Schilling M, Besselmann M, Leonhard C, Mueller M, Ringelstein EB, Kiefer R: Microglial activation precedes and predominates over macrophage infiltration in transient focal cerebral ischemia: a study in green fluorescent protein transgenic bone marrow chimeric mice. Exp Neurol 2003, 183:25–33
43. Vallierès L, Sawchenko PE: Bone marrow-derived cells that populate the adult mouse brain preserve their hematopoietic identity. J Neurosci 2003, 23:5197–5207
44. Kennedy DW, Abkowitz JL: Kinetics of central nervous system microglial and macrophage engraftment: analysis using a transgenic bone marrow transplantation model. Blood 1997, 90:986–993
45. Dillon SR, Mancini M, Rosen A, Schlissel MS: Annexin V binds to viable B cells and colocalizes with a marker of lipid rafts upon B cell receptor activation. J Immunol 2000, 164:1322–1332
46. Gundersen HJG: Stereology of arbitrary particles. A review of unbiased number and size estimators and the presentation of some new ones, in memory of William R. Thompson. J Microsc 1986, 143:3–45
47. Gundersen HJG, Bagger P, Bendtsen TF, Evans SM, Korbo L, Marcussen N, Moller A, Nielsen K, Nyengaard JR, Pakkenberg B, Sorensen FB, Vesterby A, West MJ: The new stereological tools: disector, fractionator, nucleator and point sampled intercepts and their use in pathological research and diagnosis. APMIS 1988, 96:857–881
48. Hickey WF, Kimura H: Perivascular microglial cells of the CNS are bone-marrow derived and present antigen in vivo. Science 1988, 239:290–292
49. Sjöstrand J: Proliferative changes in glial cells during nerve regeneration. Cell Tissue Res 1965, 68:481–493
50. Watson WE: An autoradiographic study of incorporation of nucleic-acid precursors by neurones and glia during nerve regeneration. J Physiol 1965, 180:741–753
51. White CA, McCombe PA, Pender MP: Microglia are more susceptible than macrophages to apoptosis in the central nervous system in experimental autoimmune encephalomyelitis through a mechanism not involving Fas (CD95). Int Immunol 1998, 10:935–941
52. Raivich G, Haas S, Werner A, Klein MA, Kloss C, Kreutzberg GW: Regulation of MCSF receptors on microglia in the normal and injured mouse central nervous system: a quantitative immunofluorescence study using confocal laser microscopy. J Comp Neurol 1998, 395:342–358
53. Tomozawa Y, Inoue T, Takahashi M, Adachi M, Satoh M: Apoptosis of cultured microglia by the deprivation of macrophage colony-stimulating factor. Neurosci Res 1996, 25:7–15